Accepted Article

Title: Ethanol and higher alcohols synthesis from syngas over CuCoM (M=Fe, Cr, Ga and Al) nanoplates derived from hydrotalcite-like precursors

Authors: Kai Sun, Yingquan Wu, Minghui Tan, Liyan Wang, Guohui Yang, Min Zhang, Wei Zhang, and Yisheng Tan

Ethanol and higher alcohols synthesis from syngas over CuCoM (M=Fe, Cr, Ga and Al) nanoplates derived from hydrotalcite-like precursors

Kai Sun,[a,b] Yingquan Wu,[a] Minghui Tan,[a] Liyan Wang,[a,b] Guohui Yang,[a] Min Zhang,[c,d] Wei Zhang,[c,d] and Yisheng Tan*[a,c]

Abstract: A series of CuCoM (M=Fe, Cr, Ga and Al) nanoplates derived from hydrotalcite-like precursors were synthesized by co-precipitation method and evaluated for ethanol and higher alcohols (HA) from syngas. The CuCoAl nanoplates demonstrated prominently improved HA selectivity of 54.9%, and the fraction of ethanol/HA reached up to 55.9% level. As revealed by XRD and HAADF-STEM results, the presence of Al species in the CuCoAl nanoplates obviously enhanced the dispersion ability of Cu and Co species. Moreover, the abundance of basic sites (surface hydroxyl groups) on CuCoAl nanoplates resulted in the formation of formate species, which was a significant C_1 species for the generation of CH_x intermediates. More importantly, a high probability of CO bridge adsorption on metallic Co atoms was found over optimized CuCoAl catalyst, which provided a favourable effect for CO dissociation, leading to the formation of CH_x intermediates. Therefore, more CH_x intermediates were generated from the formate species and CO bridge adsorption on metallic Co atoms, which provided a beneficial role for C-C chain growth in the higher alcohols production in CO hydrogenation reaction. Furthermore, a moderate ratio of surface Cu/Co was observed over optimized CuCoAl nanoplates, which can exert a synergetic effect between Cu and Co species. Ultimately, the enhanced catalytic performance was attributed to the combination of the Cu and Co species and the basic property of the CuCoAl nanoplates.

Introduction

Increasing concerns about dwindling of fossil fuel resources and soaring crude oil price have pushed the theme of energy to the center stage. In order to relieve the strong dependence on oil, the extensive and efficient employments of coal, biomass feedstock and natural gas or shale gas have aroused great interest.[1-3] Ethanol and higher alcohols (HA, $C_{2+}OH$) have been considered as clean liquid fuels (fuel additives), hydrogen carriers for fuel cell and precursors for value-added chemicals

[a]   State Key Laboratory of Coal Conversion, Institute of Coal Chemistry, Chinese Academy of Sciences, Taiyuan 030001, China;
[b]   University of Chinese Academy of Sciences, Beijing 100049, China;
[c]   China National Engineering Research Center for Coal-Based Synthesis, Institute of Coal Chemistry, Chinese Academy of Sciences, Taiyuan 030001, China;
[d]   Technology Center, Shanxi Lu'an Mining (Group) Co.Ltd., Changzhi, 046204, China
*Corresponding Author
E-mail address: tan@sxicc.ac.cn; Tel. / fax: +086-351-4044287

Supporting information for this article is given via a link at the end of the document.

and pharmaceuticals.[4-6] Production of ethanol and HA by the catalytic conversion of syngas (a mixture of H_2 and CO), derived from coal, natural gas and nonfood biomass, is one of the most promising routes for exploiting the nonoil energy friendly and efficiently.[7,8]

A wide variety of heterogeneous catalysts have been investigated in the ethanol and HA synthesis via CO hydrogenation. Generally speaking, these catalysts can be classified into four types, which are noble Rh-based catalysts, modified hydrodesulphurization catalysts (Mo/MoS$_2$-based), modified methanol synthesis (MS) catalysts (Cu-based or ZnCr-based)[9,10] and modified Fischer-Tropsch synthesis (FTS) catalysts (Co-based or Fe-based).[11,12] Investigations into the modified FTS catalysts (Co-based) have been extensively explored for ethanol and higher alcohols synthesis (HAS) through CO hydrogenation since the Institut Francais du Petrole (IFP) initially reported the CuCo catalyst in 1978.[13-16] Studies on Co-based system were principally based on Cu-containing formulations due to low raw materials price and high HA yield. The majority of scientists argued that there is a synergetic effect between copper and cobalt active sites with different roles in the CuCo catalyst, in which Co active site catalyze CO dissociation to form surface alkyl group (CH_x) species while copper active site provides non-dissociation CO adsorption and insertion.[17-19] Therefore, the intimate contact between uniformly dispersed copper and cobalt active species has been realized as a key role in the production of ethanol or HA.[17,20] Nevertheless, it is still a challenge to obtain a higher catalytic activity and HA selectivity in the complex CO hydrogenation process consisting of several side reactions (water-gas shift reaction, methanol synthesis and alkane synthesis). Besides, a wide distribution of alcohols, obeying a proximate Anderson-Schulz-Flory (ASF) distribution, was universally observed among total alcohols (C_1-C_6OH), which can bring forth a non-commercial and discommodious influence on alcohol products separation process.[21-23] Consequently, the design and optimization of CuCo catalyst with desired catalytic activity and high HA selectivity with a narrow distribution of alcohols via heterogeneous CO hydrogenation is a promising, but challenging goal.

Layered double hydroxides (LDHs), known as anionic clays or hydrotalcite-like compounds, are a class of inorganic lamellar materials with the general chemical formula $[M_{1-x}^{2+}M_x^{3+}(OH)_2]^{x+}[A^n]_{x/n} \cdot mH_2O$, where M^{2+} and M^{3+} are uniformly distributed on the atomic scale in the brucite-like layer.[24,25] More importantly, a topological transformation of LDH precursor converts to mixed metal oxides (MMO) in the calcination process of LDH precursor, which still provides a high dispersion of mixed metal oxides. Besides, LDHs have a wide range of potential applications in the basic catalysis field, resulting from the presence of abundant surface hydroxyl groups.[26] In recent years, tremendous interest has been focused attention on LDH

materials as CuCo-based catalysts for heterogeneous CO hydrogenation. The group of Liu prepared CoCu nanoparticles by calcination of the $(Cu_xCo_y)Al$-LDH (x/y=0.5) precursor, which achieved a higher CO activity and HA selectivity. As suggested by them, the small crystal size and the high surface area resulted in the excellent catalytic performance and stability.[27] Besides, the core-shell Cu@(CuCo-alloy) nanoparticles embedded on Al_2O_3 via an in situ growth of CuCoAl-LDH on Al substrates were fabricated by Gao et al. They argued that the unique electronic and geometric interaction between Cu and Co contributed to the prominent enhancement of catalytic performance.[19] Very recently, our group also explored the distinct synthesis routes, such as introduction of Cu and Co simultaneously in the LDH system, sub-impregnated Co or Cu on as-synthesized CuAl-LDH or CoAl-LDH and CuCo co-impregnated on r-Al_2O_3, to tune proximity of active phases as well as particle size, and finally uncovered the nature of synergistic catalysis of CuCo nanosheets for ethanol and HA synthesis from syngas.[20] Notably, the LDH precursors, consisting of Cu, Co and M metal ions, were calcined and subsequently reduced in situ in the fixed bed reactor to generate catalytically active species particles supported on the remaining metal oxides species (M_2O_3). Nevertheless, the role of M^{3+} elements in the CuCo-based LDH systems as the catalyst precursors was ignored currently for the design of efficient catalysts in the heterogeneous CO hydrogenation.

In this study, a series of CuCoM (M=Fe, Cr, Ga and Al) nanoplates derived from corresponding LDH precursors were synthesized and evaluated for CO hydrogenation to ethanol and higher alcohols. These samples were well characterized to investigate the influence of M^{3+} elements in the LDH systems as well as to establish the structure-performance relationship. Microstructure and morphology of catalysts were determined by XRD, SEM, HRTEM and HAADF-STEM techniques. The acid and basic properties of the catalysts affected by the CuCoM-LDH presursors were identified by temperature-programmed desorption experiment of CO_2 and NH_3 (CO_2-TPD and NH_3-TPD). In addition, the XPS and in situ DRIFT characterizations were employed to realize the surface structures and active phases of reduced catalysts.

Results and Discussion

3.1. Structural and morphological characteristics of catalysts

Figure S1a shows the XRD patterns of the CuCoFe, CuCoCr, CuCoGa and CuCoAl-LDH hydrotalcite precursors via co-precipitation (CP) method. Representative diffraction peaks at 2 theta values of 11.7°, 23.7°, 34.7°, 38.9°, 47.0°, 60.1°, 61.5° were clearly observed in all precursors, which were assigned to the characteristic features of (003), (006), (012), (015), (018), (110) and (113) basal lattice planes of hydrotalcite-like structure with 3R packing of layers, respectively.[28,29] Besides, no other crystalline impurity phase was detected in these precursors, indicating a precise control during the synthesis of hydrotalcite precursors. The position of the (110) reflection represents the

lattice parameter a, which is a function of the average distance of metal ions within the layers and indicates the density of metal ions. The lattice parameter c is related to the interlayer distance given by (003) lattice plane. The lattice parameters a and c of LDH precursors were calculated in Table S1. The lattice parameter a decreased in the order of a (CuCoFe)>a (CuCoGa)>a (CuCoCr)>a (CuCoAl), which exhibited a positive linear correlation between lattice parameter a and average radius of the cations, in agreement with the Vegard's law.[30-32] Moreover, the lattice parameter c=3d (003) was calculated to be approximately 2.2-2.3 nm, indicating the interlayer anion was CO_3^{2-} in every LDH system. The mixed metal oxides were developed after the parent CuCoM-LDH precursors were calcined at 400 °C for 5 h in the still air.
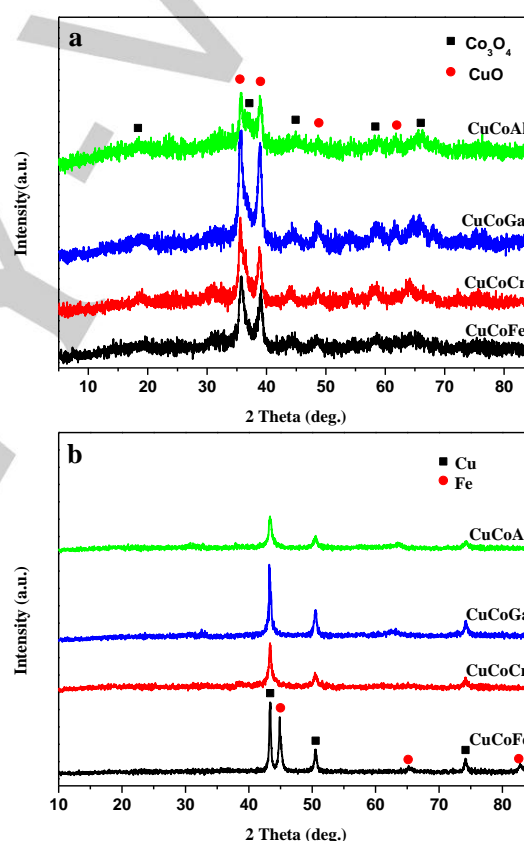
**Figure 1.** The XRD patterns of the (a) calcined catalysts and (b) spent catalysts.

As shown in Figure 1a, the typical reflection peaks of CuCoM-LDH precursors thoroughly disappeared accompanied by the presence of diffraction peaks for mixed metal oxides. For all calcined CuCoM catalysts, the reflection peaks at 2 theta = 35.6°, 38.9° and 2 theta = 18.4, 37.1°, 45.1°, 58.5°,65.5° were assigned to CuO (JCPDS 65-2309) crystalline phase and Co_3O_4 spinel structure (JCPDS 65-3103), respectively. Compared with calcined CuCoFe, CuCoCr and CuCoGa catalysts, the weakest

reflection peaks of CuO phase and Co_3O_4 spinel were obviously observed over the calcined CuCoAl catalyst, indicating the increase of CuO and Co_3O_4 dispersion promoted by Al species. For all reduced samples in Figure S1b, the obvious diffraction peaks of metallic Cu phase (JCPDS 04-0836) were observed at 2 theta values of 43.4°, 50.5° and 74.5°. As for reduced and spent CuCoFe samples, the diffraction reflections at 44.82°, 65.4° and 82.7° were indexed to the metallic Fe phase (JCPDS 87-0722). In addition, no apparent diffraction peaks of Co species were found in all reduced CuCoM samples, suggesting the uniform dispersion of Co species after reduction. Compared with other reduced CuCoM (M=Fe, Cr and Ga) catalysts, the weakest diffraction peaks of metallic Cu phase were observed over reduced CuCoAl catalyst, indicating a higher dispersion of metallic Cu. This trend is similar to previous result for the calcined catalyst system. As shown in Figure 1b, the spent CuCoM catalysts all exhibited the same phase and analogous intensities in comparison to their reduced samples, which indicated that the metallic Cu nanoparticles were not obviously aggregated after reaction.

The morphologies of CuCoM-LDH hydrotalcite precursors were characterized by SEM. As shown in Figure S2, large amounts of randomly oriented plate-like microcrystals with a size of 0.17-0.57 µm and 0.19-0.78 µm were observed in the CuCoFe-LDH and CuCoGa-LDH precursors. Besides, no evident nanosheet structure was found in the CuCoCr-LDH precursor, resulting from a poor organized crystal structure, in agreement with the XRD result. Notably, numerous plate-like nanosheets with a homogeneous size of 0.11-0.26 µm were clearly observed in the CuCoAl-LDH precursor. This phenomenon indicated that the uniform size of nanoflakes materials may attribute to the well-organized dispersion of Cu, Co and Al atoms in the layers. Additionally, the corresponding EDX spectra of the detected red square area in the CuCoAl-LDH precursor and the elemental composition are shown in Figure S2e. The obtained Cu:Co:Al ratio is 2:1:1.1, which is approximately coherent with primal ratio of metal salt solutions. Unquestionably, the slight deviation between expected formula and detected ratio was extremely common in the LDH preparation.[33] The plate-like morphologies of CuCoM (M=Fe, Ga, Al)-LDH precursors were partially aggregated after calcinations at 400 °C in Figure S3(a-d). In order to further reveal the special microstructures of calcined CuCoAl catalyst, TEM and HAADF-STEM characterization techniques were performed.

As can be seen from Figure 2a and 2c, large amounts of closed-packed plate-like nanosheets were observed in the calcined CuCoAl sample. Meanwhile, a narrow particle size distribution (4-9 nm) with the peak value at 7 nm of the calcined CuCoAl catalyst suggested a homogeneous dispersion of mixed CuCo oxides nanoparticles. Moreover, the high-resolution TEM (HRTEM) image of calcined CuCoAl catalyst (Figure 2b) revealed the existence of two interlayer spacing of 0.23 nm and 0.47 nm within two adjacent nanoparticles, which were attributed to the lattice planes of CuO (111) and Co_3O_4 (111), respectively.[34] In addition, the elemental mappings of calcined CuCoAl catalyst decided by HAADF-STEM and the relevant

EDX technique presented a homogeneous dispersion of Cu, Co, Al and O elements, which resulted from a close proximity and strong interaction of these elements.
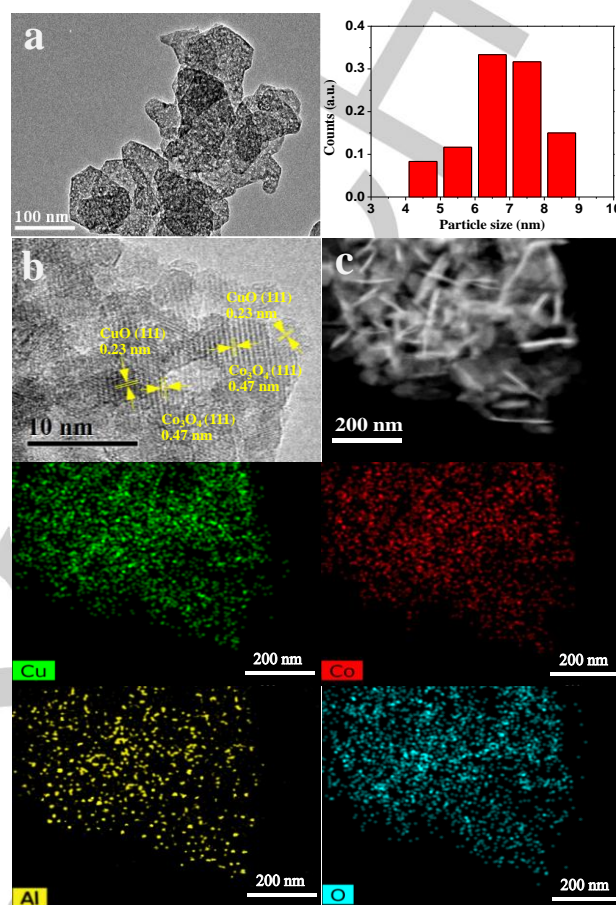
Figure 2. TEM and HRTEM images (a,b) and the particle size distribution of calcined CuCoAl catalyst; (c) HAADF-STEM image of calcined CuCoAl catalyst and the corresponding EDX element mapping images of Cu, Co, Al and O.

3.2. Evaluation of catalytic performance

As shown Table 1, a series of CuCoM (M=Fe, Cr, Ga, Al) catalysts were used to evaluated their catalytic performance in the CO hydrogenation tests under conditions of 270 °C, 2.5 MPa, GHSV = 7500 h^{-1}, and H_2/CO = 2. Compared with other CuCoM (M=Fe, Cr Ga) catalysts, the CuCoAl catalyst displayed a slightly higher catalytic activity with CO conversion of 36.2%, a prominently higher total alcohols selectivity (ROH) of 40.7% and a lower hydrocarbon selectivity of 57.5%. The CuCoFe catalyst produced a slightly higher selectivity of alkane (61.6%) including a high methane fraction of 36.0%. As for CuCoCr catalyst or CuCoGa catalyst, a much higher selectivity of hydrocarbon (more than 67%) with the large amount of C_{2+} alkanes as the main products was observed. The above results indicated the presence of Al species in CuCo-based catalyst improved both the catalytic activity and alcohol selectivity. The CO_2 selectivity over all CuCoM catalysts was less than 5.0%, indicating that the

Table 1. Catalytic performance of the catalysts in CO hydrogenation reaction.

Catalyst	CO Conv.(%)	Selectivity (C mol %)					Alcohols distribution (C mol %)				
		CH₄	C₂₊H	DME	CO₂	ROH	MeOH	EtOH	PrOH	BuOH	C₅₊OH
CuCoFe	32.3	36.0	25.6	1.7	4.6	32.1	59.4	25.8	10.7	3.4	0.8
CuCoCr	30.5	22.1	44.9	6.2	0.5	26.3	69.6	18.7	7.9	2.5	1.3
CuCoGa	27.8	29.9	41.1	4.1	4.3	20.6	82.7	11.8	4.0	1.3	0.2
CuCoAl	36.2	24.0	33.5	1.3	0.5	40.7	45.1	30.7	14.6	8.0	1.6

Reaction conditions: Fixed bed, T= 270 °C, P= 2.5 MPa, GHSV=7500 h⁻¹, n(H₂): n(CO)=2:1.
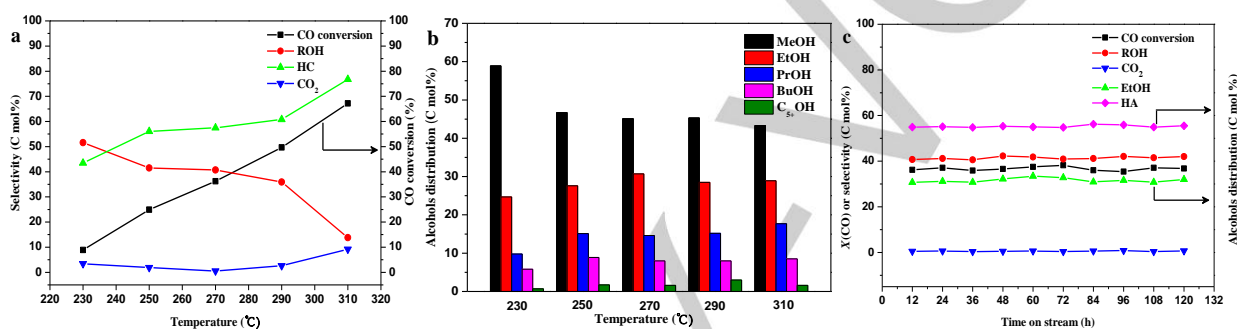
Figure 3. (a) Influence of reaction temperature on the performance of CuCoAl catalyst, (b) alcohols distribution at different reaction temperature over CuCoAl catalyst and stability test for optimized CuCoAl catalyst with reaction time on stream at T=270 °C, P=2.5 MPa, GHSV=7500 h⁻¹ and H₂/CO=2/1. Note: the DME selectivity was not shown in the product distribution.

CuCo active sites inhibited the occurrence of water-gas shift reaction and ensured the high carbon resource utilization efficiency. As far as the alcohols distribution was concerned, the fraction of methanol was more than 59.4% in total alcohols over CuCoM (M=Fe, Cr and Ga) catalysts, suggesting the poor carbon chain growth probability of alcohols in the higher alcohols synthesis (HAS). However, a much higher fraction of higher alcohols (HA) was 54.9% over CuCoAl catalyst, and the fraction to ethanol/HA reached up to 55.9% level. Considering both alcohols selectivity in all products and ethanol fraction in alcohols distribution, the CuCoAl catalyst demonstrated a relatively good catalytic performance in CO hydrogenation to ethanol and HA.

Moreover, the influence of reaction temperature from 230 °C to 310 °C on the catalytic performance of optimized CuCoAl catalyst was investigated (Figure 3a,b). As shown in Figure 3a, as the temperature increasing from 230 to 310 °C, the CO conversion enhanced remarkably to the maximum value of 67.2% at 310 °C. Nevertheless, the alcohols selectivity (ROH) descended slightly from 230 to 290 °C, and then decreased dramatically to 13.8% at 310 °C. The selectivity of hydrocarbons was opposite to that of alcohols. Although a higher selectivity of total alcohols (51.6%) was observed at 230 °C, the relatively low ethanol fraction (24.7%) and HA fraction (41.1%) were obtained over the CuCoAl catalyst. With the temperature increasing, the ethanol fraction presented a volcanic curve with maximum value of 30.7% at 270 °C (Figure 3b). Accordingly, the reaction

temperature of 270 °C was a proper condition to produce ethanol and HA over optimized CuCoAl catalyst. Besides, the stability test of CuCoAl catalyst was performed and shown in Figure 3c. As shown in Figure 3c, no evident reduction of CO conversion and total alcohols selectivity were observed in the 120 h catalytic run. Meanwhile, the fractions of ethanol and HA among total alcohols remained nearly unperturbed until the end of the stable test. These results suggest that the CuCoAl nanoplates catalyst has a good catalytic stability in CO hydrogenation reaction.

The Anderson-Schulz-Flory (ASF) distributions plots of hydrocarbons and alcohols over CuCoFe, CuCoCr, CuCoGa and CuCoAl catalysts were exhibited in Figure S4. The chain lengthening probability α value for alcohols was 0.45 over the CuCoAl catalyst, which was much higher than other CuCoM (M=Fe, Cr and Ga) catalysts. The higher α value for alcohols indicated that CuCoAl catalyst was more favourable for the production of higher alcohols. Moreover, when the number of carbon is 2, the four CuCoM catalysts present the remarkable discrepancies in the fractions of alcohols and hydrocarbons. Specifically speaking, the CuCoAl catalyst exhibited a much higher fraction of alcohols than that of hydrocarbons. The other CuCoM (M=Fe, Cr and Ga) catalyst showed that the fraction of alcohols was not higher than that of hydrocarbons. These results indicated that the CuCoAl catalyst had a greater CO insertion probability than chain lengthening probability, thus leading to the higher ethanol selectivity in the CO hydrogenation reaction.

Consequently, the uniform dispersion of Cu and Co nanoparticles, promoted by Al species, enhanced the synergistic effect between Cu and Co active sites, which resulted in a high probability for synthesis of ethanol and higher alcohols.

3.3. Analysis and discussion of structure-activity relationship

For the sake of uncovering the inherent structure-activity relationship existing in the CuCoFe, CuCoCr, CuCoGa and CuCoAl catalysts, systematized characterization techniques consisted of ICP-AES, N_2 adsorption desorption, NH_3-TPD, CO_2-TPD, H_2-TPR, XPS and in situ CO DRIFT were performed. As shown in Table S2, the ICP analysis of the calcined CuCoM (M=Fe, Cr, Ga and Al) catalysts showed that the content of residual Na was extremely low (less than 0.01 wt %). It has been reported that residual Na content less than 0.2 wt % does not expect to exert any significant effect on catalytic performance of CuCo catalysts.[35-37] Hence, the influence of residual Na was not investigated in detail in this paper.

As shown in Figure S5, the N_2 adsorption-desorption isotherms and corresponding pore size distribution profiles of calcined CuCoM catalysts were recorded. According to the IUPAC regulation, these isotherms all present a typical adsorption curve of type-IV with H_3-type hysteretic loop in Figure S5a, indicating the presence of mesoporous structure.[28] Figure S5b exhibits the distributions of pore size for calcined CuCoM catalysts. The calcined CuCoCr catalyst presented a single pore size of 15 nm, and other calcined CuCoM (M=Fe, Ga and Al) all showed dual pore sizes of 5 nm and ~50 nm, respectively. Nevertheless, the higher probability of nearly 50 nm pore size was observed over calcined CuCoAl catalyst, which may exert a favorable role on diffusion of higher alcohols molecules. Besides, compared with other calcined CuCoM (M=Fe, Cr and Ga) catalysts, a larger average pore size of 24.1 nm was observed over calcined CuCoAl catalyst (Table S2). The above results suggested that the introduction of trivalent Al elements into the LDH system would enlarge the pore size of the catalyst.
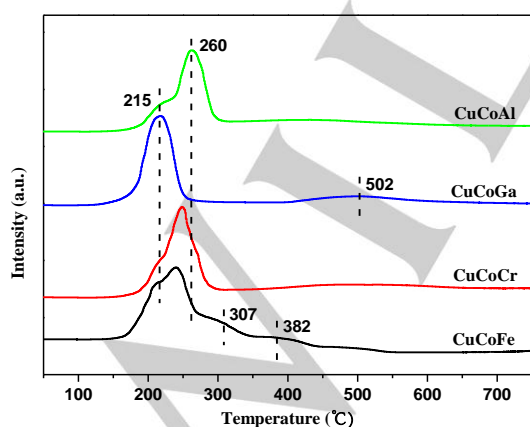

Figure 4. H_2-TPR profiles of the catalysts.

Due to illuminate the redox property and the interaction between mixed metal oxides, H_2 temperature-programmed reduction (H_2-TPR) profiles of the catalysts are recorded in Figure 4. As for CuCoGa catalyst, a symmetrical reduction peak centered at 215 °C and a weak broad reduction peak at 502 °C were observed, which ascribed to the reduction of CuO and CoGa mixed oxides, respectively. No obvious reduction peak at more than 500 °C was observed, and only a low reduction peak in the temperature range of 200 °C-260 °C was found over CuCoFe, CuCoCr and CuCoAl catalysts. The lower shoulder peak at 215 °C and the higher main reduction peak at ~260 °C were observed, which ascribed to the reduction of high dispersion of surface CuO phase and bulk CuO nanoparticle, respectively.[38] Compared with CuCoFe and CuCoCr catalysts, the highest reduction temperature (260 °C) of bulk CuO phase was observed over CuCoAl catalyst, indicating the strongest interaction force between CuO species and Al_2O_3 species. Furthermore, as for CuCoFe catalyst, the weak broad reduction peaks at 307 °C and 382 °C were displayed, which attributed to the two reduction stages of $Fe_2O_3 \rightarrow Fe_3O_4 \rightarrow Fe$.[39] On the whole, the H_2-TPR characterization provided the direct information about strong interaction between Cu active species and Al species over the CuCoAl catalyst, which may promote the dispersion of CuO phase and affect electronic structure of Cu species.
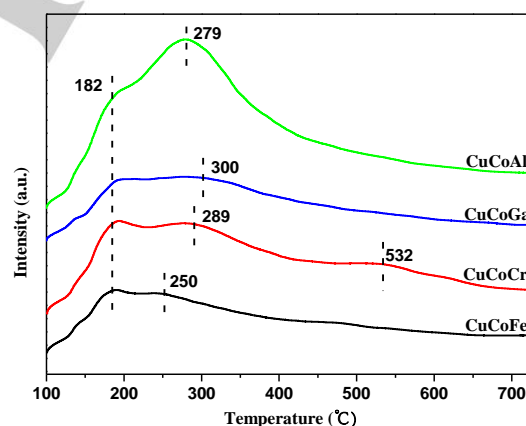

Figure 5. NH_3-TPD profiles of the calcined catalysts.

It is acknowledged that the mixed oxides acquired via thermal treatment of LDH precursors possess several acid and basic active sites. The acidic properties of the in situ reduced CuCoM catalysts were investigated by NH_3-TPD measurements (Figure 5). Three main types NH_3 desorption peaks at 182 °C, 250-300 °C and 532 °C were observed, which attributed to the weak acid sites, medium acid sites and strong acid sites, respectively. In addition to large amounts of weak acid sites at 182 °C and few medium acid sites at 289 °C, a spot of strong acid sites at 532 °C were observed over CuCoCr sample. As for

other CuCoM (M=Fe, Ga and Al) catalysts, weak acid sites and medium acid sites were observed, and no obvious strong acid sites at were detected. The CuCoFe catalyst showed the lowest density of acidity, indicating that Fe species prominently decreased the acidic property, in agreement with the work of Khodakov.[40] Remarkably, the abundant medium acid sites at 279 °C and a handful of weak acid sites were found in the CuCoAl catalyst. Previous researches by Cosimo et al.[41] on the NH_3 desorption on Al_2O_3 support showed that aluminium oxide contained the Bronsted acid sites (weak acid sites) and Lewis acid sites (medium-strength acid sites or strong acid sites). The medium-strength acid sites or strong acid sites adsorbed NH_3 by coordinating the N free electron pair with Al^{3+}, whereas on weak acid sites the surface proton was donated to NH_3 with the synthesis of NH_4^+. According to the description of Cosimo, the medium acid sites in the CuCoAl catalyst acted as the medium-strength Lewis acid sites, which were generated from Al^{3+}. Besides, Tan et al.[42] have reported that the acidic property of the samples was a key factor for the alcohols synthesis, and the medium acid sites improved the selectivity of higher alcohols. In a word, the CuCoAl catalyst exhibited highest density of medium acid sites, which significantly enhanced the selectivity of higher alcohols in CO hydrogenation reaction.
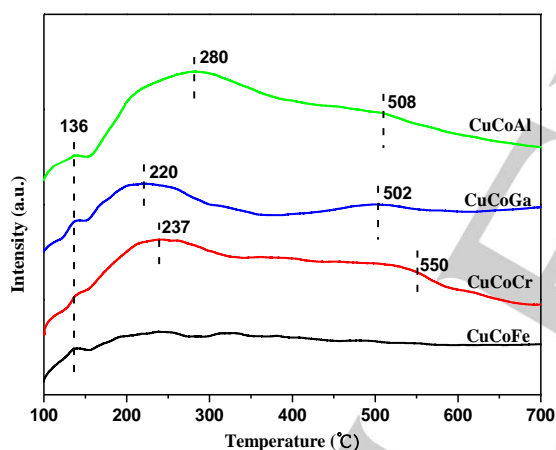

Figure 6. CO_2-TPD profiles of the calcined catalysts.

The basic properties of the CuCoM catalysts were determined by CO_2-TPD characterization (Figure 6). As for CuCoM (M=Cr, Ga and Al) catalysts, three CO_2 desorption peaks at 136 °C, 220-280 °C and 502-550 °C were displayed, which ascribed to the weak basic sites, medium-strength basic sites and strong basic sites, respectively. Just as the acidic property of CuCoFe catalyst, only weak basic sites were exhibited at low temperature. However, the selectivity of higher alcohols of was higher than that of CuCoGa or CuCoCr catalyst, but was lower than that of CuCoAl catalyst. This indicated that the acid-basic property of catalyst was not the only reason for the synthesis of higher alcohols. Besides, unlike other M species (Cr, Ga and Al), the Fe species itself was the active site for the

C-C chain growth. Namely, the improvement of ethanol or higher alcohols selectivity was caused by the combination of the active sites (Cu and Co species) of the catalyst and the acidity-basicity of the catalyst. According to the opinion of Marcu et al.,[43] the weak basic sites were associated with surface OH groups; medium-strength basic sites were relevant to M^{3+}-O^{2-} acid-base pairs, and strong basic sites were related to the existence of low coordinated O^{2-}. Compared with CuCoCr or CuCoGa catalyst, much more basic sites, especially medium-strength basic sites, derived from Al^{3+}-O^{2-} acid-base pairs, were observed over the CuCoAl catalyst surface. Some authors argued that the enhancement of basic sites can stabilize oxygenate species, directing the formation toward alcohols rather than hydrogenations.[44] Moreover, Pokrovski and Tan et al.[45-47] found that the formation of formate species, involving the migration of a proton from a surface OH group (basic sites) to adsorbed CO, was a significant C_1 intermediate for higher alcohols synthesis. Tokunaga et al.[48] also reported that large amounts of basic sites can inhibit several side reactions such as isomerization, coke deposition and dehydration. Summarizing, abundant basic sites on optimized CuCoAl catalyst may involve the generation of a C_1 species (formate species), resulting in the enhancement of CH_x intermediates, and thus promote the formation of higher alcohols. Besides, the presence of formate species will be discussed in the following section.

To further investigate the compositions and oxidation states of surface active species of these catalysts, the XPS spectra were collected. The Cu 2p XPS spectra of calcined CuCoFe, CuCoCr, CuCoGa and CuCoAl catalysts surface in Figure S6a displayed two main peaks centered at ca. 954.0 eV and 934.2 eV, corresponding to Cu $2p_{1/2}$ peak and Cu $2p_{3/2}$ peak, respectively, as well as the 2p→3d satellite peak between 940 and 945 eV, which confirmed that Cu species existed as Cu^{2+} with a d^9 configuration.[49] Co 2p photoemission spectra for all calcined catalysts are exhibited in Figure S6b. The spin-orbit doublets of Co $2p_{1/2}$ peak and Co $2p_{3/2}$ peak of the calcined catalysts were observed at around 795.2 eV and 780.4 eV, respectively, and no obvious satellite peak was found, suggesting that the presence of Co_3O_4 spinel.[50] After the reductive activation procedure, the XPS spectra of Cu 2p binding energy (BE) for CuCoFe, CuCoCr, CuCoGa and CuCoAl samples were recorded in Figure S7. The Cu $2p_{3/2}$ BE of reduced catalysts shifted down to lower value around 932.4 eV and the satellite peaks between 945 and 940 eV vanished in comparison with calcined catalysts, indicating that Cu^{2+} species was reduced to lower oxidation state (Cu^+ or Cu^0) species.[28,51] Besides, the distinction of Cu^+ or Cu^0 species was achieved via Cu LMM X-ray Auger electron spectroscopy (XAES) spectra of reduced catalysts in Figure 7. It was observed that the broad and asymmetrical peak can be deconvoluted into two ratio of symmetrical peaks centered at around 918 eV and 916 eV, which was assigned to Cu^0 and Cu^+, respectively.[28,52] Furthermore, a modified Cu Auger parameters (α'_{Cu}), which represents the summation of BE of Cu $2p_{3/2}$ and KE of Cu LMM Auger electron, were calculated in Table 2. As shown in this table, the values of α'_{Cu} between 1850.5 and 1851.0 eV were attributed to the presence of Cu^0. The values of α'_{Cu} were in the

range of 1848.7 to 1849.1 eV, which can be assigned to the existence of Cu^+.[53] From the deconvolution of Cu LMM peak results, a gradually enhanced ratio of surface $Cu^+/(Cu^++Cu^0)$ for reduced samples was observed in the order CuCoGa < CuCoCr < CuCoFe < CuCoAl, in agreement with the enhancement of ethanol selectivity. This result indicated that a higher ratio of Cu^+ may be beneficial to non-dissociation CO insertion on the catalyst surface; thus, the selectivities of ethanol and higher alcohols improved in the CO hydrogenation reaction. Besides, a higher ratio of surface Cu^+ was found over reduced CuCoAl sample, which may attribute to a stronger interaction between Cu and Al species, in agreement with H_2-TPR result. The ratios of surface $Cu^+/(Cu^++Cu^0)$ of CuCoM (M=Fe, Cr and Ga) catalysts decreased obviously after reaction. However, a slightly reduced ratio of surface Cu^+ was observed over spent CuCoAl catalyst (Table 2), indicating the Cu^+ species on the CuCoAl nanoplates surface was steady during the reaction.
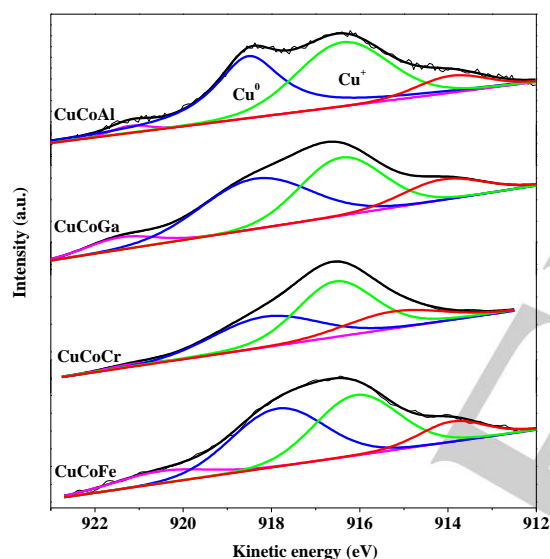
Figure 7. Cu LMM XAES spectra of reduced CuCoFe, CuCoCr, CuCoGa and CuCoAl catalysts.

Table 2. Cu species on the reduced and spent CuCoFe, CuCoCr, CuCoGa and CuCoAl catalysts derived from Cu LMM XAES spectra.

Catalyst	KE (eV)		α' (Cu)		X_{Cu}^+ (%)		Cu/Co[c]
	Cu^0	Cu^+	Cu^0	Cu^+			
CuCoFe	917.8	915.9	1850.6	1848.7	49.0[a]	45.8[b]	1.22
CuCoCr	918.0	916.4	1850.5	1848.9	47.4	43.3	1.30
CuCoGa	918.3	916.4	1851.0	1849.1	46.6	40.7	0.35
CuCoAl	918.5	916.4	1851.0	1848.9	50.7	50.2	1.15

[a] Intensity ratio between Cu^+ and (Cu^0+Cu^+) by deconvolution of Cu LMM XAES spectra over reduced catalysts.
[b] Intensity ratio between Cu^+ and (Cu^0+Cu^+) over spent catalysts.
[c] Surface Cu/Co molar ratios of reduced catalysts.

As shown in Figure S8, two obvious satellite peaks of Co 2p were displayed at 803.0 eV and 786.5 eV, suggesting the existence of Co^{2+} from the reduction of Co_3O_4. Besides, the corresponding binding energy of Co $2p_{1/2}$ and Co $2p_{3/2}$ moved slightly toward higher values at 796.7 eV and 780.7 eV, which also certified the reduction of Co_3O_4. The difference in binding energy between CoO and Co_3O_4 is extremely small, but the energy gap (ΔE) between Co 2p spin-orbit doublets enables it possible to identify them. Specifically speaking, ΔE value is 15.0 eV for Co_3O_4, and is 15.7-15.9 eV for CoO.[54,55] As for all reduced CuCoM (M=Fe, Cr, Ga and Al) samples, ΔE values are ca. 15.9 eV, suggesting the existence of Co^{2+} instead of Co^{3+}. Deconvolution of the Co $2p_{3/2}$ peaks over reduced CuCoFe, CuCoCr, CuCoGa and CuCoAl samples showed binding energy at ca. 782.2 eV, 780.4 eV and 778.4 eV, which were ascribed to $Co(OH)_2$, CoO and Co^0, respectively.[55] The existence of $Co(OH)_2$ was attributed to the interaction between Co^{2+} and catalyst surface OH group. Quantitative results about the surface Co species of reduced CuCoFe, CuCoCr, CuCoGa and CuCoAl samples from Co $2p_{3/2}$ XPS spectra are shown in Table S3. A gradually decreased Co^0 content for reduced catalysts was observed in the order of CuCoAl > CuCoFe > CuCoCr > CuCoGa, agreeing with the decrease of CO conversion.
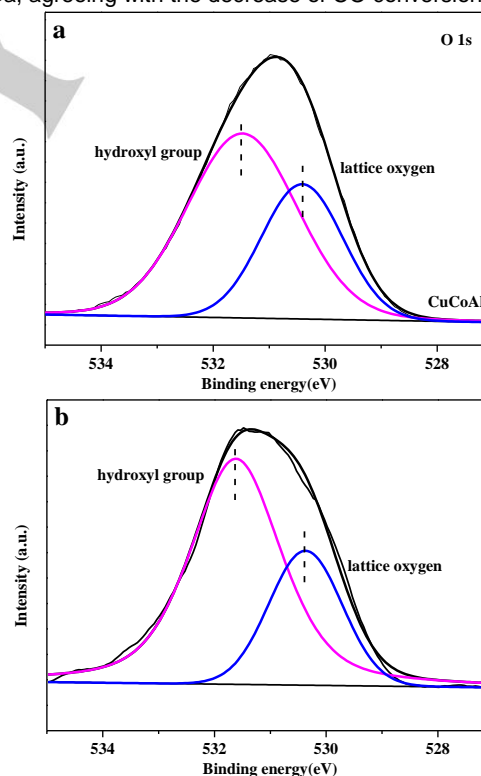
**Figure 8.** O 1s peaks of (a) reduced and (b) spent CuCoAl catalyst.

The O 1s peaks of reduced and spent CuCoAl catalyst are shown in Figure 8. The broad O 1s peak can be deconvoluted into two symmetrical peaks centered at 531.5 eV and 530.4 eV,

which was assigned to surface hydroxyl group and lattice oxygen, respectively.[42] The molar ratio of OH/(OH+O_{latt}) over reduced CuCoAl sample was 65.80%, which was calculated on the basis of corresponding peaks areas. A large amount of surface OH groups were derived from weak basic sites of the CuCoAl catalyst. Therefore, it was concluded that the formation of formate species may be related to involvement of surface hydroxyl groups. Besides, compared with the reduced catalyst, the molar ratio of OH/(OH+O_{latt}) (69.2%) on the surface of the spent catalyst was slightly enhanced (Figure 8b), which indicated that OH groups seem to be stable or regenerative during the reaction.

Table 2 shows the surface Cu/Co molar ratios of the reduced CuCoM catalysts. Seen from the data listed in Table 2, a higher ratio of surface Cu/Co was observed over reduced CuCoFe or CuCoCr sample, which resulted in a higher selectivity of methanol among total alcohols. Furthermore, the reduced CuCoGa sample exhibited a lower surface Cu/Co, which led to an enhancement of hydrocarbons. As for reduced CuCoAl catalyst, a moderate ratio of surface Cu/Co (1.15) was found, which can exert a synergetic effect between Cu and Co species, and thus maintained the balance interplay of both CO insertion and C-C chain growth probability.

To acquire further insight into surface sensitive message, in situ CO DRIFT technique (Figure 9) was used to reveal the surface active sites and adsorbed species of CuCoM catalysts. As shown in Figure 9, under the initial Ar atmosphere (1 min),

two evident adsorption peaks at 2172 and ca. 2111 cm^{-1} were observed over all reduced catalysts, which were attributed to gas phase CO.[56] However, under the continuous evacuation of gas phase CO for 3-9 min, the CO adsorption peak at higher value of 2172 cm^{-1} gradually vanished, whereas the peak centered at ca. 2111 cm^{-1} initially decreased (3 min) in size but remained unchangeable in size in the following time (5, 7 and 9 min). It has been reported that the stronger interaction and thermal stability of CO with Cu^+ sites compared with that of Cu^0 or Cu^{2+}.[28,57] Therefore, the stable peak at ca. 2111 cm^{-1} for each CuCoM catalyst was assigned to the CO adsorption on Cu^+ species. Besides, compared with CuCoFe and CuCoGa samples, the CuCoAl sample showed a slight lower value of CO adsorption (red-shift), resulting from an electronic donor and acceptor interaction between Cu and Al_2O_3 species improved the electron density of Cu species.[28] Notably, the peaks were observed at 1577 cm^{-1} and ca. 1354 cm^{-1} over CuCoCr and CuCoAl catalysts associated with the vibration modes of v_{as} (OCO) and δ (CH) of bidentate formate species (b-HCOO).[45,58,59] The formation of bidentate formate species attributed to the interaction between absorbed CO and surface basic sites (OH groups or O^{2-}) on the CuCoCr or CuCoAl catalyst surface, in agreement with large amounts of basic sites of the two catalysts. Besides, a large amount of surface OH groups were found over reduced CuCoAl catalyst in previously
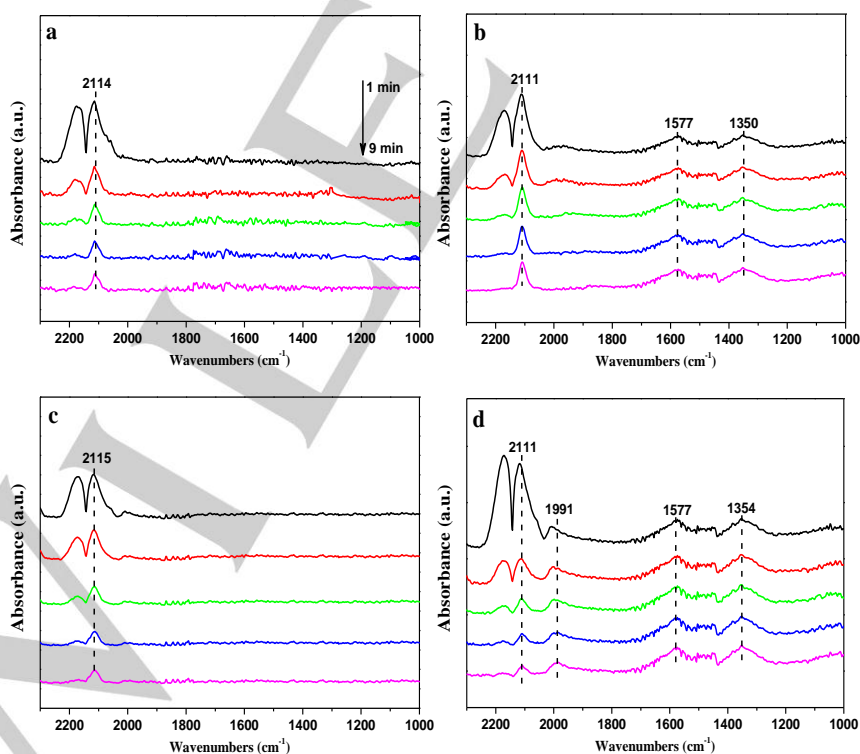
Figure 9. In situ CO DRIFT spectra over reduced catalysts under Ar flow at room temperature for 1 min, 3 min, 5 min, 7 min and 9 min of (a) CuCoFe; (b) CuCoCr; (c) CuCoGa and (d) CuCoAl catalysts.

mentioned XPS result. For the sake of acquiring accurate information about the change of hydroxyl content under CO atmosphere, the background spectrum of reduced CuCoAl sample was recorded before the introduction of CO (Figure S9).

As shown in Figure S9, a series of broad reversal peaks at around 3400 cm^{-1} were observed under CO flow, indicating a consumption of hydroxyl groups.[46] At the same time, the intensities of v_{as} (OCO) and δ (CH) for formate species (b-HCOO) increased. Consequently, the formation of formate species can relate to involvement of surface OH groups on CuCoAl nanoplates surface. Subsequently, the CuCoAl sample was exposed to H$_2$ flow for several minutes, and the corresponding spectrum were recorded. Under the H$_2$ atmosphere, the intensities of peaks related to formate species decreased, while the reversal peak of consumed OH groups decreased and gradually became flat. This phenomenon indicated the OH groups can be reproduced by formate species (HCOO) hydrogenation on CuCoAl nanoplates surface. Therefore, the consumption and generation of OH groups was a dynamic equilibrium during the reaction, which was also consistent with the O XPS analysis.
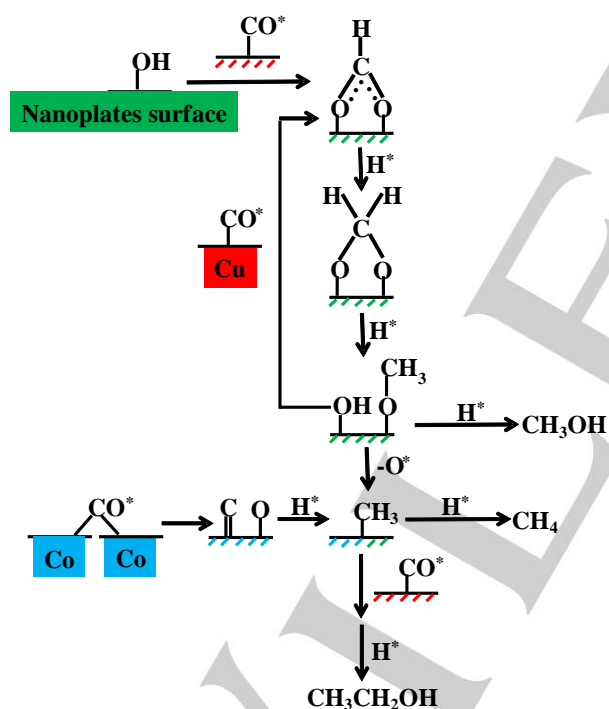
Figure 10. The reaction scheme for the formation of methanol, methane and ethanol from syngas on CuCoAl nanoplates.

Some authors[45-47,60] have reported that the formation of formate species (b-HCOO) is a key C$_1$ species for higher alcohols synthesis. However, the specific route of higher alcohols synthesis from syngas via formate species is still unclear so far. In view of the catalytic performance and characterization results mentioned above, a simple reaction mechanism that explains the formation of methanol, methane and ethanol from syngas on CuCoAl nanoplates is proposed in Figure 10. Firstly, the formation of formate species (HCOO) involved the reaction of OH groups on nanoplates surface with CO* on Cu active site. Subsequent steps comprised step-wise hydrogenation of HCOO to H$_2$COO intermediates, H$_2$COO intermediates to CH$_3$O and OH groups. Meanwhile, the refilled OH groups on nanoplates surface can continue to react with CO* to form HCOO. Hence, the circulation of OH groups was observed over CuCoAl nanoplates surface during CO hydrogenation reaction. In the following step, the C-O cleavage of resulting CH$_3$O was found to give CH$_x$ intermediates. Meanwhile, the CO bridge adsorption on metal Co active sites was found at 1991 cm^{-1} over CuCoAl sample (Figure 9d), resulting in an easier cleavage of C-O bond, and thus promoted the generation of CH$_x$ intermediates.[20] Therefore, the CH$_x$ intermediates were generated from the formate species and CO bridge adsorption on metallic Co atoms. Finally, the produced CH$_x$ intermediates coupled to CO* to generate CH$_x$CO, which was continually hydrogenated to ethanol. In a word, the synergetic catalysis of CuCo active sites and abundant basic sites (hydroxyl groups) on CuCoAl nanoplates are responsible for synthesis of ethanol and higher alcohols.

Conclusions

In conclusion, a series of CuCoM (M=Fe, Cr, Ga and Al) nanoplates derived from corresponding LDH precursors were successfully fabricated and evaluated for CO hydrogenation to ethanol and higher alcohols. The catalytic activity and higher alcohols selectivity depended sensitively on the CuCo active sites and acidic-basic sites of catalysts. The CuCoAl catalyst exhibited evident enhancement of catalytic performance compared to other CuCoM (M=Fe, Cr and Ga) catalysts. The combination of systematic characterizations and catalytic performance was applied to explain the improved catalytic performance of CuCoAl catalyst. The uniform dispersion of Cu and Co species over CuCoAl nanoplates was confirmed by XRD and HAADF-STEM characterizations. Besides, abundant basic sites (mainly hydroxyl groups) on CuCoAl nanoplates were found by CO$_2$-TPD, XPS and in situ CO DRIFT characterization, which can involve the formation of formate species. More importantly, a high probability of CO bridge adsorption on metallic Co atoms was detected over CuCoAl catalyst, resulting in enhancement of CH$_x$ intermediates. In brief, the CH$_x$ intermediates were generated from the formate species and CO bridge adsorption on metallic Co atoms, which were indispensable C$_1$ intermediates for higher alcohols production. Additionally, a higher ratio of Cu$^+$ of CuCoAl sample, derived from a strong interaction between Cu and Al species, was observed by XPS technique. It may be beneficial to non-dissociation CO insertion on the catalyst surface, and thus promotes the formation of higher alcohols in the CO hydrogenation reaction. The investigation uncovers the role of

active sites and acid-base property of the catalysts in the synthesis of ethanol and higher alcohols.

Experimental Section

Catalyst preparation

Synthesis of the CuCoM-LDH (M=Fe, Cr, Ga and Al) precursors

The CuCoM (M=Fe, Cr, Ga and Al) precursors with identical chemical compositions ((Cu+Co)/M=3, Cu/Co=2/1) were synthesized by co-precipitation (CP) method. In a representative preparation procedure, a mixed solution (A) containing 9.66 g $Cu(NO_3)_2 \cdot 3H_2O$, 5.82 g $Co(NO_3)_2 \cdot 6H_2O$ and 7.50 g $Al(NO_3)_3 \cdot 9H_2O$ was dissolved in 300 mL deionized water. A aqueous solution (B) was obtained by dissolving 5.16 g NaOH and 4.40 g Na_2CO_3 in 300 mL deionized water. Afterwards, the two aqueous solutions of A and B were added to the three-necked flask simultaneously at a constant rate of 5 mL min^{-1} under continual magnetic stirring at 85 °C for 24 h. The obtained precipitation was washed thoroughly with deionized water and ethanol for several times, and finally dried in the oven at 60 °C overnight. The CuCoFe, CuCoCr and CuCoGa-LDH precursors were prepared by using the same preparation route.

Calcination of catalyst precursors

All catalyst samples were synthesized by calcination of the precursor at 400 °C for 5 h (heating rate of 1°C min^{-1}) in the muffle furnace.

Catalyst characterization techniques

Powder X-ray diffraction (XRD) data for the samples were collected on a Rigaku D/max 2500 diffractometer with Cu Kα radiation (λ=0.1546 nm). The instrument was operated at 40 kV voltage and 40 mA current within the range of scattering angle 2 theta of 5-85° at a speed of 4° min^{-1}. The morphology and microstructures of the precursors and catalysts were recorded on a JSM-7001F scanning electron microscope (SEM) instrument coupled to energy dispersive X-ray spectroscopy (EDX) at 15 kV accelerating voltage and 10 mA current. Transmission electron microscopy (TEM) and high resolution transmission electron microscopy (HRTEM) equipped with a high-angle annular dark-field scanning-transmission electron microscopy (HAADF-STEM) and energy dispersive X-ray spectroscopy (EDX) mappings were taken using a JEOL JEM-2100F instrument at 200 kV operating voltage. Prior to the measurement, the catalyst powder was ultrasonically dispersed in ethanol, and then supported on a carbon film coated 200 mesh Mo grid. Temperature-programmed reduction with hydrogen (H_2-TPR) was conducted on a TP-5080 programmed chemisorption instrument (Tianjin Xianquan Corporation). 0.03 g of the calcined catalyst sample was sandwiched between two pieces of quartz wool inside the TPR quartz tube. Then, the quartz tube was inserted into the chemisorption instrument. The catalyst was pre-treated under N_2 flow at the rate of 30 mL min^{-1} at 200 °C for 1 h before cooling to room temperature. After the pre-treatment, the reduction process was treated in a 10% H_2/N_2 flow of 30 mL min^{-1} with the temperature ramping up from room temperature to 800 °C at the speed of 5 °C min^{-1}. Temperature-programmed desorption experiment of NH_3 (NH_3-TPD) or CO_2 (CO_2-TPD) was performed on a TP-5080 programmed chemisorption instrument equipped with a TCD detector. Before the adsorption process of NH_3 or CO_2, 0.10 g catalyst was pre-treated under N_2 atmosphere (30 mL min^{-1}) at 200 °C for 1 h to remove physically adsorbed water. After cooling to 100 °C, the sample was exposed to NH_3

or CO_2 flow for 1 h after pre-treatment at 400 °C for 1 h in 10% H_2/N_2 flow. Finally, the profile of NH_3-TPD or CO_2-TPD was recorded from 100 °C to 800 °C at a ramping rate of 5 °C min^{-1} in the N_2 flow. The N_2-physisorption measurement of the catalyst was performed on Quantachronr SI series setup. The X-ray photoelectron spectroscopy (XPS) and Auger electron spectroscopy (XAES) measurements on the AXIS ULTRA DLD instrument were carried out using a 1486.6 eV Kα aluminium X-ray source under ultrahigh vacuum (<10^{-6} Pa). The binding energy scale of the spectrometer was calibrated using the adventitious C1s binding energy at 284.6 eV. The concentration of each element was obtained from the area of corresponding peak. Besides, in order to acquire the XPS information of reduced catalyst, the fresh catalyst was reduced in a flow of 10% H_2/N_2 atmosphere at 400 °C for 1 h in the pre-treatment instrument. After that, the system pressure attained 10^{-8} Pa, and then the reduced catalyst entered into analytic cell, and finally all elemental photoelectron lines were recorded. In situ diffuse reflectance infrared Fourier transform (DRIFT) spectra were collected (64 averaged scans, with a resolution of 4 cm^{-1}) on a Bruker Tensor 27 spectrometer. A liquid nitrogen cooled mercury cadmium telluride (MCT) detector was employed. Before each measurement, 20 mg calcined sample was put into an in situ analysis cell with KBr windows. Above all, the sample was reduced online at 400 °C for 1 h in a 10% H_2/N_2 atmosphere and evacuated for 30 min at this temperature. After the temperature dropped to 270 °C with a background spectrum recorded under Ar flow. Subsequently, the gaseous CO was swarmed into the in situ cell at 270 °C for 30 min with the spectrum recorded. Finally, the sample was flushed with Ar at the room temperature for 30 min. Selected spectrum of the reduced sample was collected under CO and Ar flow. Residual Na content was obtained by Inductively Coupled Plasma Atomic Emission Spectroscopy (ICP-AES) technique using Thermo iCAP6300.

Catalytic test in CO hydrogenation reaction

The CO hydrogenation catalytic reaction was carried out with a stainless steel fixed-bed reactor (15 mm in inner diameter, 23 mm in outside diameter and 500 mm in length) using a 1.5 g calcined catalyst (30-40 mesh). At the fixed-bed reactor outlet, a condensing unit was installed to separate the gas phase and liquid phase products. Prior to each test, the calcined catalyst was in situ reduced at 400 °C for 5 h under atmospheric pressure with 10% hydrogen-in-nitrogen mixture stream (30 mL min^{-1}). Subsequently, the temperature was decreased and held at desired temperatures (270-310 °C) and the reactor was pressurized to 2.5 MPa with the synthesis gas feedstock mixture ($H_2/CO=2$). Flow rate of synthesis gas was controlled by a mass flow meter to gain a gas hourly space velocity (GHSV) of 7500 mL g_{cat}^{-1} h^{-1}. Catalytic activity and products selectivities were acquired after 12 h of steady state on account of composition of gas and liquid products. The carbon balance was in the range of 98-101% for all tests.

The exhaust gas stream (H_2, CO, CH_4 and CO_2) was online analyzed by GC4000A apparatus with a carbon molecular sieves column and a thermal conductivity detector (TCD) with Ar as the carrier gas. The organic gas products (C_1-C_5 hydrocarbons) were detected online in a GC4000A device with GDX-403 column connected to a flame ionization detector (FID) with N_2 as the carrier gas. The aqueous and liquidus methanol products were analyzed by a GC4000A with a GDX-401 column and a thermal conductivity detector (TCD) with Ar as the carrier gas. Total alcohol products (methanol, ethanol and propanol, et al.) in the liquid phase were analyzed by a GC-7AG with a Chromosorb 101 column and a flame ionization detector (FID) with N_2 as the carrier gas.

FULL PAPER

[1] V. Subramani, S.K. Gangwal, Energy Fuels 2008, 22, 814-839.
[2] A. Corma, *Chem. Rev.* **2014**, *114*, 1545-1546.
[3] T.J. Morgan, R. Kandiyoti, *Chem. Rev.* **2014**, *114*, 1547-1607.
[4] H.M. Torres Galvis, J.H. Bitter, C.B. Khare, M. Ruitenbeek, A.I. Dugulan, K.P. de Jong, *Science* **2012**, *335*, 835-838.
[5] S. Chu, A. Majumdar, *Nature* **2012**, *488*, 294.
[6] L. Wang, L. Wang, J. Zhang, X. Liu, H. Wang, W. Zhang, Q. Yang, J. Ma, X. Dong, S.J. Yoo, J.G. Kim, X. Meng, F.S. Xiao, *Angew. Chem., Int. Ed.,* **2018**, *130*, 6212-6216.
[7] T.Y. Chen, J. Su, Z. Zhang, C. Cao, X. Wang, R. Si, X. Liu, B. Shi, J. Xu, Y.F. Han, *ACS Catal.* **2018**, *8*, 8606-8617.
[8] H.T. Luk, C. Mondelli, S. Mitchell, S. Siol, J.A. Stewart, D. Curulla Ferré, J. Pérez-Ramírez, *ACS Catal.* **2018**, *8*, 9604-9618.
[9] Y. Wu, H. Xie, S. Tian, N. Tsubaki, Y. Han, Y. Tan, *J. Mol. Catal. A: Chem.* **2015**, *396*, 254-260.
[10] L. Tan, G. Yang, Y. Yoneyama, Y. Kou, Y. Tan, T. Vitidsant, N. Tsubaki, *Appl. Catal. A-Gen.* **2015**, *505*, 141-149.
[11] M. Ao, G.H. Pham, J. Sunarso, M.O. Tade, S. Liu, *ACS Catal.* **2018**, *8*, 7025-7050.
[12] H.T. Luk, C. Mondelli, D.C. Ferré, J.A. Stewart, J. Pérez-Ramírez, *Chem. Soc. Rev.* **2017**, *46*, 1358-1426.
[13] X. Ning, Z. An, J. He, *J. Catal.* **2016**, *340*, 236-247.
[14] G.R. Johnson, S. Werner, A.T. Bell, *ACS Catal.* **2015**, *5*, 5888-5903.
[15] P. Wang, S. Chen, Y. Bai, X. Gao, X. Li, K. Sun, H. Xie, G. Yang, Y. Han, Y. Tan, *Fuel* **2017**, *195*, 69-81.
[16] H.T. Luk, T. Forster, C. Mondelli, S. Siol, D. Curulla-Ferré, J.A. Stewart, J. Pérez-Ramírez, *Catal. Sci. Technol.* **2018**, *8*, 187-200.
[17] G. Prieto, S. Beijer, M.L. Smith, M. He, Y. Au, Z. Wang, D.A. Bruce, K.P. de Jong, J.J. Spivey, P.E. de Jongh, *Angew. Chem. Int. Ed.* **2014**, *53*, 6397-6401.
[18] X. Xiaoding, E.B.M. Doesburg, J.J.F. Scholten, *Catal. Today* **1987**, *2*, 125-170.
[19] W. Gao, Y. Zhao, H. Chen, H. Chen, Y. Li, S. He, Y. Zhang, M. Wei, D.G. Evans, X. Duan, *Green Chem.* **2015**, *17*, 1525-1534.
[20] K. Sun, X. Gao, Y. Bai, M. Tan, G. Yang, Y. Tan, *Catal. Sci. Technol.* **2018**, *8*, 3936-3947.
[21] V. Mahdavi, M.H. Peyrovi, M. Islami, J.Y. Mehr, *Appl. Catal. A* **2005**, *281*, 259-265.
[22] Y. Yang, X. Qi, X. Wang, D. Lv, F. Yu, L. Zhong, H. Wang, Y. Sun, *Catal. Today* **2016**, *270*, 101-107.
[23] L. Zhao, W. Li, J. Zhou, X. Mu, K. Fang, *Int. J. Hydrogen Energy* **2017**, *42*, 17414-17424.
[24] J. Yu, Q. Wang, D. O'Hare, L. Sun, *Chem. Soc. Rev.* **2017**, *46*, 5950-5974.
[25] P.J. Sideris, U.G. Nielsen, Z. Gan, C.P. Grey, *Science* **2008**, *321*, 113-117.
[26] M. Xu, M. Wei, *Adv. Funct. Mater.* **2018**, *28*, 1802943.
[27] A. Cao, G. Liu, Y. Yue, L. Zhang, Y. Liu, *RSC Adv.* **2015**, *5*, 58804-58812.
[28] J. Wu, G. Gao, P. Sun, X. Long, F. Li, *ACS Catal.* **2017**, *7*, 7890-7901.
[29] M.M.J. Li, C. Chen, T. Ayvalı, H. Suo, J. Zheng, I.F. Teixeira, L. Ye, H. Zou, D. O'Hare, S.C.E. Tsang, *ACS Catal.* **2018**, *8*, 4390-4401.

[30] K. Parida, L. Mohapatra, N. Baliarsingh, *J. Phys. Chem. C* **2012**, *116*, 22417-22424.
[31] L. Francke, E. Durand, A. Demourgues, A. Vimont, M. Daturi, A. Tressaud, *J. Mater. Chem.* **2003**, *13*, 2330-2340.
[32] V. Aubin-Chevaldonnet, D. Caurant, A. Dannoux, D. Gourier, T. Charpentier, L. Mazerolles, T. Advocat, *J. Nucl. Mater.* **2007**, *366*, 137-160.
[33] S. Li, H. Wang, W. Li, X. Wu, W. Tang, Y. Chen, *Appl. Catal. B* **2015**, *166-167*, 260-269.
[34] Y. Zhang, J. Huang, Y. Ding, *Appl. Catal. B* **2016**, *198*, 447-456.
[35] J.A. Dalmon, P. Chaumette, C. Mirodatos, *Catal. Today* **1992**, *15*, 101-127.
[36] X. Mo, Y.-T. Tsai, J. Gao, D. Mao, J.G. Goodwin, *J. Catal.* **2012**, *285*, 208-215.
[37] S. Prodinger, M.A. Derewinski, Y. Wang, N.M. Washton, E.D. Walter, J. Szanyi, F. Gao, Y. Wang, C.H.F. Peden, *Appl. Catal. B* **2017**, *201*, 461-469.
[38] Z. Boukha, J.L. Ayastuy, A. Iglesias-González, B. Pereda-Ayo, M.A. Gutiérrez-Ortiz, J.R. González-Velasco, *Appl. Catal. B.* **2014**, *160-161*, 629-640.
[39] L. Zhou, L.R. Enakonda, Y. Saih, S. Loptain, D. Gary, P. Del-Gallo, J.M. Basset, *ChemSusChem* **2016**, *9*, 1243-1248.
[40] J. Wang, P.A. Chernavskii, Y. Wang, A.Y. Khodakov, *Fuel* **2013**, *103*, 1111-1122.
[41] J.I. Di Cosimo, Apesteguı, C.R.´a, M.J.L. Ginés, E. Iglesia, *J. Catal.* **2000**, *190*, 261-275.
[42] X. Gao, Y. Wu, T. Zhang, L. Wang, X. Li, H. Xie, Y. Tan, *Catal. Sci. Technol.* **2018**, *8*, 2975-2986.
[43] O.D. Pavel, D. Tichit, I.-C. Marcu, *Appl. Clay Sci.* **2012**, *61*, 52-58.
[44] V.P. Santos, B. van der Linden, A. Chojecki, G. Budroni, S. Corthals, H. Shibata, G.R. Meima, F. Kapteijn, M. Makkee, J. Gascon, *ACS Catal.* **2013**, *3*, 1634-1637.
[45] K. Pokrovski, K.T. Jung, A.T. Bell, *Langmuir* **2001**, *17*, 4297-4303.
[46] X. Gao, T. Zhang, Y. Wu, G. Yang, M. Tan, X. Li, H. Xie, J. Pan, Y. Tan, *Fuel* **2018**, *217*, 21-30.
[47] S. Tian, S. Wang, Y. Wu, J. Gao, P. Wang, H. Xie, G. Yang, Y. Han, Y. Tan, *Catal. Sci. Technol.* **2016**, *6*, 4105-4115.
[48] T. Ishida, T. Yanagihara, X. Liu, H. Ohashi, A. Hamasaki, T. Honma, H. Oji, T. Yokoyama, M. Tokunaga, *Appl. Catal. A* **2013**, *458*, 145-154.
[49] X. Zheng, H. Lin, J. Zheng, X. Duan, Y. Yuan, *ACS Catal.* **2013**, *3*, 2738-2749.
[50] Y. Yamada, K. Yano, Q. Xu, S. Fukuzumi, *J. Phys. Chem. C* **2010**, *114*, 16456-16462.
[51] J. Gong, H. Yue, Y. Zhao, S. Zhao, L. Zhao, J. Lv, S. Wang, X. Ma, *J. Am. Chem. Soc.* **2012**, *134*, 13922-13925.
[52] Z. He, Z. Lin, P. He, Y. Yuan, *J. Catal.* **2011**, *277*, 54-63.
[53] L.F. Chen, P.J. Guo, M.H. Qiao, S.R. Yan, H.X. Li, W. Shen, H.L. Xu, K.N. Fan, *J. Catal.* **2008**, *257*, 172-180.
[54] R. Riva, H. Miessner, R. Vitali, G. Del Piero, *Appl. Catal. A* **2000**, *196*, 111-123.
[55] T. Mathew, N.R. Shiju, K. Sreekumar, B.S. Rao, C.S. Gopinath, *J. Catal.* **2002**, *210*, 405-417.
[56] M.L. Smith, N. Kumar, J.J. Spivey, *J. Phys. Chem. C* **2012**, *116*, 7931-7939.
[57] Y. Wang, Y. Shen, Y. Zhao, J. Lv, S. Wang, X. Ma, *ACS Catal.* **2015**, *5*, 6200-6208.
[58] D.S. Deutsch, A. Siani, P.T. Fanson, H. Hirata, S. Matsumoto, C.T. Williams, M.D. Amiridis, *J. Phys. Chem. C* **2007**, *111*, 4246-4255.
[59] S. Kattel, B. Yan, B. Yang, J.G. Chen, P. Liu, *J. Am. Chem. Soc.* **2016**, *138*, 12440-12450.
[60] A. Kiennemann, H. Idriss, R. Kieffer, P. Chaumette, D. Durand, *Ind. Eng. Chem. Res.* **1991**, *30*, 1130-1138.

FULL PAPER

Entry for the Table of Contents

FULL PAPER

The combination of active sites and OH groups on the CuCoAl nanoplates is the key for the efficient promotion of CO hydrogenation to ethanol and higher alcohols.
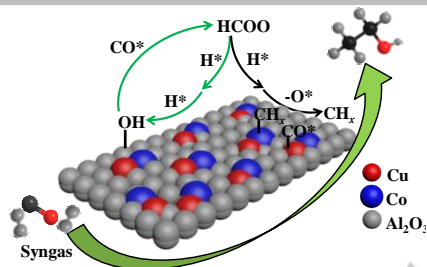
Kai Sun, Yingquan Wu, Minghui Tan, Liyan Wang, Guohui Yang, Min Zhang, Wei Zhang, and Yisheng Tan*

Page No. – Page No.

Ethanol and higher alcohols synthesis from syngas over CuCoM (M=Fe, Cr, Ga and Al) nanoplates derived from hydrotalcite-like precursors